Three-Dimensional High-Fidelity Dynamic Modelling of Tether Transportation System with Multiple Climbers

Gangqiang Li*
York University, 4700 Keele Street, Toronto, Ontario, M3J 1P3, Canada
Gefei Shi†
Northwest Polytechnical University, 127 Youyi W Rd, Beilin, Xi'an, Shaanxi, China 710072
Zheng H. Zhu‡
York University, 4700 Keele Street, Toronto, Ontario, M3J 1P3, Canada

This paper studies the dynamics of tether transportation system by the nodal position finite element method in the framework of arbitrary Lagrangian-Eulerian description. Material coordinate is introduced as state variable that is decoupled with the position coordinate. The movement of climbers is represented by moving nodes associated with the material coordinates. It is integrated into the finite element method by variable-length tether together with a process of dividing and merging elements. The dynamic behavior of tether transportation system with multiple climbers is studied. The results show that the elastic-flexible tether model is able to capture the high frequency oscillation of the tether transportation system. The oscillation could have adverse effect on the safe operation of the tether transportation system, especially in causing the fatigue failure of tether, and must be considered.

I. Introduction

* Doctoral candidate. Department of Earth and Space Science and Engineering.
† Doctoral candidate. National Key Laboratory of Aerospace Flight Dynamics, and School of Astronautics. Currently, visiting doctoral student at Department of Mechanical Engineering, York University.
‡ Professor, Department of Mechanical Engineering; gzhu@yorku.ca. AIAA Associate Fellow and lifetime member (Corresponding Author).

TETHER Transportation System(TTS) is an attractive alternative to the classical space elevator due to its ability for long-range mass transfer between two satellites at low cost [1]. TTS generally consists of a main satellite, a subsatellite, and one or multiple climbers that move along the tether for orbital transfer of payloads [2]. Due to its floating nature, TTS is prone to libration instability as the result of the Coriolis forces acting on the moving climbers.

Past decades have witnessed many studies of the TTS. Cohen and Misra [3] studied the dynamics of TTS with one climber based on the assumptions of rigid tether and two-piece dumbbell model. Since then, the influences of TTS parameters, such as, initial libration angles, mass, velocity of moving climber, and tether length, on the dynamic characteristics of TTS have been studied extensively by the two-piece dumbbell model [4, 5]. Cohen and Misra further expended the two-piece dumbbell model by considering the elasticity of tether to investigate the influence of longitudinal and transverse oscillations of tether on the libration of TTS [6]. However, the coupling mechanism of the climbers with the tether was glossily simplified by simply varying the lengths of two tether segments connected to the climber. Williams [7] replaced the two-piece dumbbell model by a lumped mass-viscoelastic-spring model. Two approaches were developed to treat the dynamics of the climber: dynamic and kinematic approaches. The dynamic approach modelled the climber as an independent lumped mass subjected to tether tensions, friction force between the tether and the climber, and the propelling force of the climber. The concept is clear and simple, but the computational load is high. The kinematic approach describes the climber motion by varying the lengths of tethers connecting to the climber, which is an extension of the work of Cohen and Misra [6]. Numerical simulation shows two approaches yield very similar results for a TTS with only one climber. Recently, Sun et al. [8] studied the dynamics of a TTS with one climber by the absolute nodal coordinate formulation. The dynamics of the climber is independently established and the coupling between the tether and the climber is achieved by

projecting the climber's velocity onto the tether with the Lagrange multiplier method.

In addition to one climber scenario, TTS with multiple climbers was also investigated. The concept of the multiple climbers with proper phase shift was first proposed to alleviate the libration of TTS in payload transfer [3]. Then, a multibody dynamic model is developed to investigate the effect of transient motion of multiple climbers on the libration of tether [2]. Furthermore, the simultaneous operation of a descending and an ascending climber is proposed to cancel the Coriolis forces acting on the tether induced by climbers [9], leading to significant reduction of tether libration. Although effective, there are still aspects of TTS with multiple climbers not fully investigated. For example, the center of mass (CM) of the TTS may shift during the transfer of payloads [4]; the coupling of longitudinal and transverse oscillations of flexible tether with moving climbers are not fully understood [3, 5]; the constraint equations that couples the motions of the tether and the climber are oversimplified [7, 8]; the out-of-plane motion is generally neglected [10], and the tether model is built at a rotational frame by implying the orbital plane being fixed spatially [7-9], just to name a few. Thus, a model of high fidelity and easy implementation is highly desired, which inevitably involves the modeling of tethers and tethered satellites with full dynamics.

Many modeling methods have been proposed to study the dynamic behavior of tethered spacecraft systems, such as, the lumped mass method [7, 9, 11, 12], finite difference method [13], Kane's method [10], modal method [6], rigid element method [14-17], absolute nodal coordinate finite element method [8], and nodal position finite element method [18-23]. Among them, the nodal position finite element method (NPFEM) is appealing due to its flexibility and capability in handling complex tether properties and boundary conditions of a TTS, and ease of implementation with existing finite element method. Moreover, the integration of moving climbers along the tether into the tether dynamics is technically challenging. Currently, there are two types of methods: the uncoupled and coupled methods. The uncoupled method is simple and straightforward. It ignores

the dynamic coupling between the tether and climber [9, 11]. Instead, the climber is replaced by a force vector moving along the tether at a given climbing velocity. The coupled method is divided into two categories in terms of the coupling techniques. The first is the sequential coupling, where the dynamics of the climber and tether are modeled separately and a constraint equation is introduced to couple the spatial position and climbing velocity of climber with the tether by the Lagrangian multiplier method [8]. However, it needs to determine the position of climber along the tether in the process. Moreover, the position of climber is projected to the undeformed state of tether for simplicity, which may be inaccurate if the tether is bent significantly [8]. The second is the true coupling, where the dynamics of climber and tether are fully modeled and solved simultaneously. To achieve this, a variable-length element model is introduced [7]. The movement of climber is represented by changing the lengths of two elements connecting to the climber with one being increasing and the other being decreasing. This approach is superior to the sequential coupling approach because it can describe not only the climber movement along the tether but also the variable length problems, such as, the tether deployment and retrieval of a TTS. Therefore, the fully coupled approach is adopted in the current work.

Two approaches exist in the variable-length element method. One is to divide the tether into constant numbers of elements, and the lengths of elements vary at the same rate. The conservation of mass and energy due to the length variation is presented [24]. Accordingly, the degree-of-freedom of the numerical model does not change, and the complex process of dividing and merging elements is avoided. However, it is only suitable for the tether deployment or retrieval problem without climbers moving along the tether [11, 16, 24-27]. The other approach uses two types of elements: the constant-length and the variable-length elements [7, 28]. The elements connected to the climbers are the variable-length elements and the rest elements are constant-length elements. Thus, it requires the continuity constraint at the interface between the variable and constant length

elements [29]. While it does provide flexibility in modeling climbers moving along the tether, the degree-of-freedom of numerical model varies due to the dividing and merging elements. However, existing method has three limitations [7]. First, the conservation of mass and energy due to the length variation is not clarified. Second, a search algorithm is needed to determine the element where the climber locates, which may fail if the tether bends significantly. Third, the method cannot be extended to the case of multiple climbers. In the current study, these three limitations are eliminated by the NPFEM together with the Arbitrary Lagrangian-Eulerian (ALE) description. To ensure the conservation of mass and energy in the presence of the length variation, a method with rigorous description of the variable-length element has been proposed by the ALE description [30, 31]. The ALE description introduces a concept of material points that do not associate with finite element nodes. As a result, the element nodes may have variable material coordinates that allow the finite element changes its position within the domain [30, 32]. This is advantageous because the continuity condition of the climber passing across tether element nodes can be easily enforced, which allows the dynamics of climber being easily integrated with the tether dynamics.

In the current work, an innovative approach is proposed to ensure the conservation of mass and energy of TTS with multiple climbers by the NPFEM in the ALE description (NPFEM-ALE), where the material coordinate is included as the state variable. The moving nodes represent the climbers, and the movement of climbers is accomplished by changing the lengths of variable-length elements connecting to the moving nodes. The material coordinates of the moving nodes follow the pre-defined trajectories of climbers. Thus, no search of the entire system is needed to determine the position of the climber. As the lengths of variable-length elements change with the moving climbers, new elements are either created or merged to avoid the lengths of variable-length elements being too long or too short. The newly proposed approach is verified by the solution of a TTS with one climber based on the classical two-piece dumbbell model in two different scenarios.

Once verified, it is used to analyze the dynamic behaviors of TTS with multiple climbers.

II. Arbitrary Lagrangian-Eulerian Formulation of Tether Transportation System

A. Coordinate Systems

Consider the TTS shown in Fig. 1. It consists of a main satellite, a sub satellite, an elastic and flexible tether connecting the two satellites, and multiple climbers moving along the tether. The TTS is subject to a central gravity and is orbiting in a circular orbit. The tether is discretized into n 2-noded straight elements with three translational degrees of freedom at each node. It should be pointed out only the axial tensile deformation of tether is considered in the current work. If the axial deformation is less than negative anywhere along the tether, the tether will be slack and the tension is assumed zero at that location. Let the number of nodes start from node 1 (main satellite) to node n+1 (sub satellite). The satellites and climbers are modeled as lumped masses with their attitude dynamics ignored. The motion of the TTS is described by three sets of coordinate systems: the global inertial frame of the Earth ($OXYZ$), the local frame of element ($otbn$) and the orbital frame ($O'X_oY_oZ_o$). The origin of the global inertial coordinate system is located at the Earth center. The *X-axis* points to the direction of vernal equinox, the Z-axis aligns with the Earth rotation axis and points to the North, and the Y-axis completes a right-hand coordinate system. The local coordinate system of element is defined at the element level with the origin o located at the i-th node. The t-axis is aligned with the element and pointing from i-th node to (i+*1*)-th node, the n-axis is perpendicular to the t-axis and the average velocity of two nodal velocities, and the b-axis completes a right-hand coordinate system. The orbital coordinate system is used to describe the libration motion of the TTS, and it will be defined later.

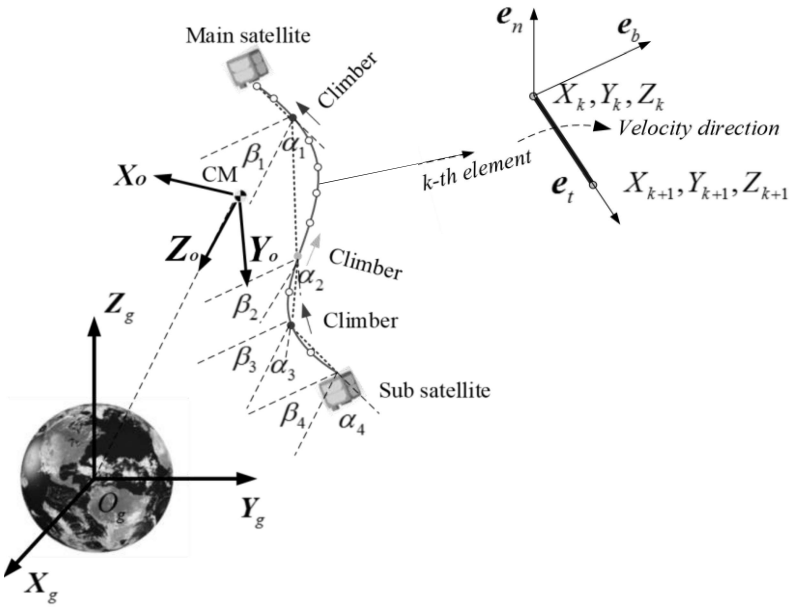

Fig. 1. Schematic of TTS system with multiple climbers.

B. Nodal Position Finite Element in Arbitrary Lagrangian-Eulerian Description

Consider the *k-th* tether element. The position of an arbitrary point inside the element can be expressed by a linear interpolation with nodal coordinates,

$$\boldsymbol{X} = \boldsymbol{N}_{a,k}\boldsymbol{X}_{a,k} \tag{1}$$

where $\boldsymbol{X}_{a,k} = \left(X_k, Y_k, Z_k, X_{k+1}, Y_{k+1}, Z_{k+1}\right)^T$ is the vector of element nodal coordinates and $\boldsymbol{N}_{a,k}$ is the shape function matrix [19, 21],

$$\boldsymbol{N}_{a,k} = \left[\frac{1-\xi}{2}\boldsymbol{I}_{3\times3}, \frac{1+\xi}{2}\boldsymbol{I}_{3\times3}\right] \tag{2}$$

where $\boldsymbol{I}_{3\times3}$ is the 3×3 identity matrix and $\xi \in [-1,1]$ denotes the dimensionless parameter.

Next, define a material coordinate p of an arbitrary point inside the k-th element as,

$$p = \frac{1-\xi}{2}p_k(t) + \frac{1+\xi}{2}p_{k+1}(t) \quad -1 \le \xi \le 1 \tag{3}$$

where $p_k(t)$ and $p_{k+1}(t)$ are the time varying material coordinates associated with the nodal points k and k+1. Then, ξ can be expressed by the material coordinates [31],

$$\xi = \frac{2p - p_k(t) - p_{k+1}(t)}{p_{k+1}(t) - p_k(t)} \tag{4}$$

Therefore, Eq. (1) can be rewritten in term of material and position coordinates, as

$$\boldsymbol{X} = \boldsymbol{N}_{a,k}\left[p, p_k(t), p_{k+1}(t)\right]\boldsymbol{X}_{a,k} \tag{5}$$

The associated velocity and acceleration of this point can be derived as,

$$\dot{\boldsymbol{X}} = \boldsymbol{N}_{a,k}\dot{\boldsymbol{X}}_{a,k} + \frac{\partial \boldsymbol{N}_{a,k}}{\partial t}\boldsymbol{X}_{a,k} = \boldsymbol{N}_{e,k}\dot{\boldsymbol{X}}_{e,k} \tag{6}$$

$$\ddot{\boldsymbol{X}} = \frac{d}{dt}\left[\boldsymbol{N}_{a,k}\dot{\boldsymbol{X}}_{a,k} + \left(\frac{\partial \boldsymbol{N}_{a,k}}{\partial p_k}\dot{p}_k + \frac{\partial \boldsymbol{N}_{a,k}}{\partial p_{k+1}}\dot{p}_{k+1}\right)\boldsymbol{X}_{a,k}\right] = \boldsymbol{N}_{e,k}\ddot{\boldsymbol{X}}_{e,k} + \boldsymbol{a}_{p,\mathrm{k}} \tag{7}$$

$$\boldsymbol{a}_{p,\mathrm{k}} = 2\left(\frac{\partial \boldsymbol{N}_{a,k}}{\partial p_k}\dot{p}_k + \frac{\partial \boldsymbol{N}_{a,k}}{\partial p_{k+1}}\dot{p}_{k+1}\right)\dot{\boldsymbol{X}}_{a,k} + \left(\frac{\partial^2 \boldsymbol{N}_{a,k}}{\partial p_k^2}\dot{p}_k^2 + 2\frac{\partial^2 \boldsymbol{N}_{a,k}}{\partial p_k \partial p_{k+1}}\dot{p}_k\dot{p}_{k+1} + \frac{\partial^2 \boldsymbol{N}_{a,k}}{\partial p_{k+1}^2}\dot{p}_{k+1}^2\right)\boldsymbol{X}_{a,k} \tag{8}$$

where $\boldsymbol{N}_{e,k} = \left(\boldsymbol{N}_{a,k}, \frac{\partial \boldsymbol{N}_{a,k}}{\partial p_k}\boldsymbol{X}_{a,k}, \frac{\partial \boldsymbol{N}_{a,k}}{\partial p_{k+1}}\boldsymbol{X}_{a,k}\right)$ is the extended shape function matrix, $\boldsymbol{X}_{e,k} = \left(\boldsymbol{X}_{a,k}^T, p_k, p_{k+1}\right)^T$ is the extended vector of nodal coordinate, $\dot{\boldsymbol{X}}_{e,k}$ and $\ddot{\boldsymbol{X}}_{e,k}$ are the extended vectors of velocity and acceleration respectively, and $\boldsymbol{a}_{p,\mathrm{k}}$ is the additional term associated with rate of material coordinates at both ends of the *k-th* element [31].

Based on the D'Alembert's principle, the sum of the virtual work done by the inertial and applied forces on the virtual displacements of TTS should be zero at an arbitrary moment, that is,

$$\delta W_{e,k} + \delta W_{g,k} - \delta W_{i,k} = 0 \tag{9}$$

where $\delta W_{e,k}$, $\delta W_{g,k}$, and $\delta W_{i,k}$ are the virtual work done by external, gravity, and inertial forces:

$$\delta W_{e,k} = -\int \delta \boldsymbol{\varepsilon}^T \boldsymbol{\sigma} A_k dp = -\int_{p_k}^{p_{k+1}} A_k \delta \boldsymbol{\varepsilon}^T \boldsymbol{\sigma} dp = -\delta \boldsymbol{X}_{e,k}^T \boldsymbol{Q}_{e,k} \tag{10}$$

$$\delta W_{g,k} = \int \delta \boldsymbol{X}_{e,k}^T \boldsymbol{f}_{g,k} A_k dp = \int_{p_k}^{p_{k+1}} \delta \boldsymbol{X}_{e,k}^T \boldsymbol{f}_{g,k} A_k dp = \delta \boldsymbol{X}_{e,k}^T \boldsymbol{Q}_{g,k} \tag{11}$$

$$\delta W_{i,k} = \int \delta \boldsymbol{X}_{e,k}^T \rho_k A_k \ddot{\boldsymbol{X}} dp = \int_{p_k}^{p_{k+1}} \delta \boldsymbol{X}_{e,k}^T \rho_k A_k \ddot{\boldsymbol{X}} dp = \delta \boldsymbol{X}_{e,k}^T \left(\boldsymbol{M}_{e,k} \ddot{\boldsymbol{X}}_{e,k} + \boldsymbol{Q}_{p,k} \right) \tag{12}$$

where ρ and A are the material density and cross-section area of element respectively, $\delta \boldsymbol{X}$ is the virtual displacement where the symbol δ represents the variational operator, the subscript k denotes the *k-th* element, $\boldsymbol{\sigma}$ and $\boldsymbol{\varepsilon}$ are the vectors of stress and strain respectively, and $\boldsymbol{f}_{g,k}$ is the vector of gravity per unit length.

Substituting Eqs. (10)-(12) into Eq. (9) yields the dynamic equations of the *k-th* element in the global inertial coordinate system [18],

$$\boldsymbol{M}_{e,k} \ddot{\boldsymbol{X}}_{e,k} = \boldsymbol{Q}_{e,k} + \boldsymbol{Q}_{g,k} - \boldsymbol{Q}_{p,k} \tag{13}$$

$$\boldsymbol{M}_{e,k} = \frac{p_{k+1} - p_k}{2} \int_{-1}^{1} \rho_k A_k \boldsymbol{N}_{e,k}^T \boldsymbol{N}_{e,k} d\xi \tag{14}$$

$$\boldsymbol{Q}_{e,k} = \frac{p_{k+1} - p_k}{2} \int_{-1}^{1} E_k A_k \varepsilon \left(\frac{\partial \varepsilon}{\partial \boldsymbol{X}_{e,k}} \right)^T d\xi \tag{15}$$

$$\boldsymbol{Q}_{g,k} = \frac{p_{k+1} - p_k}{2} \int_{-1}^{1} \boldsymbol{N}_{e,k}^T \boldsymbol{f}_{g,k} d\xi \tag{16}$$

$$\boldsymbol{Q}_{p,k} = \frac{p_{k+1} - p_k}{2} \int_{-1}^{1} \rho_k A_k \boldsymbol{N}_{e,k}^T \boldsymbol{a}_{p,k} d\xi \tag{17}$$

where E is the elastic modulus of tether, $\boldsymbol{M}_{e,k}$ is the extended mass matrix of element, $\boldsymbol{Q}_{e,k}$ and $\boldsymbol{Q}_{g,k}$ are the vectors of the elastic and gravitational forces respectively, and $\boldsymbol{Q}_{p,k}$ is the additional force caused by the mass flow of the material points, which is associated with variation of the material coordinate of k-th element.

It should be noted that there are two major differences between the newly proposed NPFEM-ALE and the existing NPFEM [18]. First, the extended mass matrix $\boldsymbol{M}_{e,k}$ of *k-th* element is no longer a constant matrix as it is in the NPFEM. The rank of $\boldsymbol{M}_{e,k}$ is six while its dimension is 8

× 8, which indicates that the normal solver does not work because it inverses the mass matrix [19, 21]. The rank deficient matrix can be decomposed into six parts as listed in Appendix A. Second, there is an additional inertial term $\boldsymbol{Q}_{p,k}$ generated by the length variation of element. It can be decomposed into five parts, and their detailed expressions are shown in Appendix B.

The elastic force is assumed the axial deformation of tether obeys the Green strain, such that,

$$\varepsilon = \frac{1}{2}\left(\boldsymbol{X}'^{T}\boldsymbol{X}' - 1\right) = \frac{1}{2}\left[\left(\frac{2}{p_{k+1} - p_k}\right)^2 \boldsymbol{X}_{a,k}^{T}\left(\frac{\partial \boldsymbol{N}_{a,k}}{\partial \xi}\right)^{T}\left(\frac{\partial \boldsymbol{N}_{a,k}}{\partial \xi}\right)\boldsymbol{X}_{a,k} - 1\right] \tag{18}$$

where $(\ )'$ denotes the first order derivative with respect to ξ.

Substituting Eq. (18) into (15) yields the elastic force vector $\boldsymbol{Q}_{e,k} = \left(\boldsymbol{Q}_{e,k}^{1}, \boldsymbol{Q}_{e,k}^{2}, \boldsymbol{Q}_{e,k}^{3}\right)^{T}$. The detailed expressions of these components are shown in Appendix C.

Finally, the dynamic equations of the motion of TTS can be obtained by assembling Eq. (13) with the standard assembly procedure in the finite element method [18, 19],

$$\boldsymbol{M}_e \ddot{\boldsymbol{X}}_e = \boldsymbol{Q}_e + \boldsymbol{Q}_g - \boldsymbol{Q}_p \tag{19}$$

where $\boldsymbol{M}_e$ is the extended and rank deficient mass matrix of TTS, $\ddot{\boldsymbol{X}}_e$ is the acceleration vector of extended nodal position of tether, $\boldsymbol{Q}_e$, $\boldsymbol{Q}_g$, and $\boldsymbol{Q}_p$ are the vectors of elastic, gravitational, and time-varying material coordinate induced forces. It should be noted the internal damping of the tether is not considered due to the lack of experimental data in space. Nonetheless, the damping effect generally suppresses the disturbance to the TTS. Thus, the neglect of damping will not affect the validation of current investigation. Finally, the material coordinate of tether increases monotonically from the first node (main satellite) to the (n+1)-*th* node (sub satellite).

C. Coupling of climbers with tether motion

The coupling of climber with tether motion is achieved by enforcing a constraint kinematically

between the tether and the climber. Assume a moving node is assigned to the position of the climber, in which the material coordinate is allowed to move along the tether to represent a climber. The two elements connecting with this moving node are defined as the variable-length elements, one increases while the other decreases. Therefore, the changing rate of material coordinate of the moving node represents the velocity of climber. Accordingly, a constraint equation can be introduced to represent the motion of the climber along the tether. For the TTS with $q \geq 1$ climbers, the constraint equations of these climbers are defined as,

$$C_{1,j}(p,t) = p_j - p_{j,\text{desired}} = 0 \quad (j = 1,2,\ldots q) \quad \text{or} \quad \boldsymbol{C}_1(p,t) = \boldsymbol{0} \tag{20}$$

where $p_{j,\text{desired}}$ denotes the pre-defined or desired position of the j-th climber.

Except for the moving node, the rest nodes are normal nodes with zero velocity of their material coordinates. The corresponding constraint equations of these nodes $(n+1-q)$ are defined as,

$$C_{2,j}(p,t) = \dot{p}_j = 0 \ (j = 1,2,\ldots n+1-q) \quad \text{or} \quad \boldsymbol{C}_2(p,t) = \boldsymbol{0} \tag{21}$$

Combining Eqs. (19)-(21) together yields the dynamic equations of the motion of TTS,

$$\begin{cases} \boldsymbol{M}_e \ddot{\boldsymbol{X}}_e + \left(\dfrac{\partial \boldsymbol{C}_1}{\partial \boldsymbol{X}_e}\right)^T \boldsymbol{\lambda}_1 + \left(\dfrac{\partial \boldsymbol{C}_2}{\partial \boldsymbol{X}_e}\right)^T \boldsymbol{\lambda}_2 = \boldsymbol{Q}_e + \boldsymbol{Q}_g - \boldsymbol{Q}_p \\ \boldsymbol{C}_1(p,t) = \boldsymbol{0} \\ \boldsymbol{C}_2(p,t) = \boldsymbol{0} \end{cases} \tag{22}$$

where $\boldsymbol{\lambda}_{1,2}$ denote the vectors of Lagrange multipliers with subscripts 1 and 2 representing the corresponding constraint equations.

D. Merging and dividing elements

As shown in Fig. 2, the lengths of variable-length elements change when the moving node moves. The variable-length element will be divided if its length is too long, or merged with the adjacent

constant-length element to form a new variable-length element if its length is too short. Four parameters are defined to control the merging and/or dividing process: the standard length L_s, the upper bound length L_{max}, the low bound length L_{min}, and the acceptance tolerance δ_e, respectively. There are two general rules to determine the values of L_{max} and L_{min}. First, the lengths of variable-length elements cannot be too short or too long, which means the values should be close to the standard length L_s. Second, the constraint condition $L_{\min} + L_{\max} > 2L_s$ should be satisfied. The purpose for this condition is to avoid the process of merging and dividing elements happening simultaneously, which may lead to an abrupt oscillation in solution.

1. Merging elements

If the length of the variable-length element is smaller than the lower bound length L_{min}, it will be merged with the adjacent constant-length element. For example, as shown in Fig. 2(a), the (k+2)-*th* node is a moving node that represents the climber moving in the arrow direction. If the following equation is satisfied,

$$L_{k+1} = p_{k+2} - p_{k+1} \le L_{\min} \tag{23}$$

the (k+2)-*th* node is ready to be merged with (k+1)-*th* node. The actual merge occurs once the condition $\|\Delta \boldsymbol{r}\| \le \delta_e$ is satisfied, where $\Delta \boldsymbol{r}$ is the normal distance from (k+1)-*th* node to the line connecting the *k-th* and (k+2)-*th* nodes. $\delta_e = 0.01\ m$ is the tolerance to avoid the oscillation caused by the merge of node. Then the nodes and elements are renumbered after (k+1)-*th* node is removed.

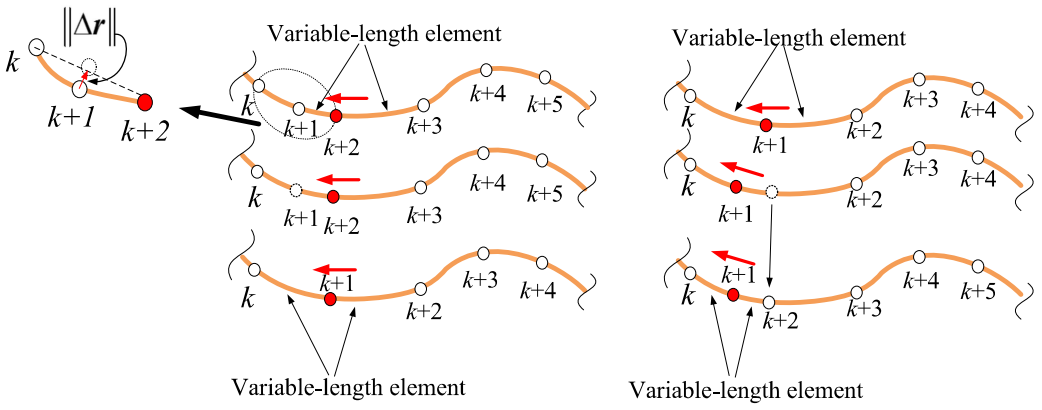

(a) **(b)**

Fig. 2. (a) Merging element. (b) Dividing element.

2. Dividing elements

The variable-length element will be divided if the element's length exceeds the upper bound length L_{max}. For example, as shown win Fig. 2(b), the (*k*+1)-*th* node is a moving node that represents the climber moving in the arrow direction. If the following condition is satisfied,

$$L_{k+1} = p_{k+2} - p_{k+1} \geq L_{\max} \tag{24}$$

the (*k*+1)-*th* element will be divided into two new elements by inserting a new node between the (*k*+1)-*th* and (*k*+2)-*th* nodes. The position, velocity, and acceleration of the newly inserted node is obtained via interpolation. Then, the nodes and elements after the (*k*+1)-*th* node are renumbered. Due to its connection with the moving node, the new (*k*+1)-*th* element is a variable-length element with the length $L_{k+1} - L_s$. The new (*k*+2)-*th* element is a constant-length element with the standard length L_s. The property of this element, either constant-length or variable-length, is depending on whether the original (*k*+2)-*th* node is a normal or moving node in case of multiple climbers.

E. Libration motion of TTS

The libration motion of the TTS is normally described in the orbital coordinate system [1-5], as shown in Fig. 3. The origin *O'* of the coordinate system is located at the center of mass (CM) of the TTS with the Z_o-axis pointing to the origin of the global inertial coordinate system. The X_o-

axis is lying in the orbital plane of TTS system and perpendicular to the Z_o-axis. The Y_o-axis completes a right-hand system. The transformation matrix from the orbital frame to the global inertial frame is the same as Ref. [21]. Different from the two-piece dumbbell model [4, 5], there are n sets of libration (pith and roll) angles if the tether is discretized into n elements. To keep consistence with the definition of libration angles of the two-piece dumbbell model, a series of virtual libration angels are defined by straight lines connecting the main satellite, the climbers, and the sub satellite, see the dotted lines in Fig. 1. Taking the case of three climber as an example, there are four dotted lines. The libration angles of those four lines are described in the orbital frame with the origin located at the CM of discretized model of TTS. The calculations of the in-plane angles $\alpha_i\,(i=1,\ldots,4)$ and out-of-plane angles $\beta_i\,(i=1,\ldots,4)$ are the same as in Refs [21, 33].

$$\begin{aligned}\alpha_i &= \tan^{-1}\left(\boldsymbol{R}_{X_o,i}/\boldsymbol{R}_{Z_o,i}\right),\\ \beta_i &= \tan^{-1}\left[-\boldsymbol{R}_{Y_o,i}/(\boldsymbol{R}_{Z_o,i}\cos\alpha_i+\boldsymbol{R}_{X_o,i}\sin\alpha_i)\right]\end{aligned} \tag{25}$$

where $\boldsymbol{R}_i=\left(\boldsymbol{R}_{X_o,i},\boldsymbol{R}_{Y_o,i},\boldsymbol{R}_{Z_o,i}\right)^T$ is the vector of a dotted line expressed in the orbital coordinate system with the subscript $i(1\sim 4)$ representing the sequence of these four lines.

III. Results and Discussion

In the current work, the backward formulation is employed together with the Newton-Raphson iteration method to solve the dynamic equations of the motion of TTS [27, 30]. The maximum iteration numbers and error tolerance of each iteration step are set as 10 and 10^{-11}, respectively. The physical properties of the tether are listed in Table. 1, and other parameters will be given later.

Table 1 Physical properties of tether.

Parameters	Values
Material density of tether (kg/m^3)	1440
Elastic modulus of the tether ($10^9 N/m^2$)	72
Cross-section area (m^2)	2.0×10^{-6}

A. Validation of the proposed approach

The proposed approach is validated by comparing the dynamic responses against to those in the Refs. [4, 5], in which the TTS contains only one climber. For the sake of comparison, the tether is discretized into two variable-length elements so that the definition of libration angles of current approach is the same as those in the Refs. [4, 5]. Moreover, the degrees-of-freedom of the TTS model is constant as the climber moves along the tether.

First, the total mass of the subsatellite m_s, the climber m_c, and the tether m_t is assumed negligible compared with the mass of the main satellite m_{m}. Thus, the CM of the TTS resides approximately at the main satellite in the transfer period of climber. The main satellite is orbiting in a circular orbit. The initial conditions and physical parameters in [17] are used here: $r(0) = 6{,}600\ km$, $\psi(0) = 1.177 \times 10^{-3}\ rad/s$, $\alpha_1(0) = \alpha_2(0) = \dot{\alpha}_1(0) = \dot{\alpha}_2(0) = 0$ $L = 100\ km$, $m_s = 1000\ kg$, $m_c = 1000\ kg$. The climber is assumed to move at a constant velocity $\dot{p}_{1,\mathrm{desired}} = 14.99\ m/s$. Both upward and downward movements of the climber are analyzed, where $l_1(0) = 0.90L$ and $l_2(0) = 0.10L$ for the upward movement, $l_1(0) = 0.10L$ and $l_2(0) = 0.90L$ for the downward movement. The transfer time is 5,336s. The comparisons of the libration motion and trajectory of the climber are shown in Figs. 3-6. Since the definition of the orbital coordinate system is different, the results from Ref. [17] are transformed into the current orbital coordinate system. Figs. 3 and 4 show the comparisons of the climber in the upward transfer, while Figs. 5 and 6 show the comparisons of the climber in the downward transfer. It is observed that both the libration angles and trajectory of the climber are in very good agreement with the results of two-piece dumbbell model in Ref. [17]. In addition, as shown in Figs. 3 and 5, the in-plane motion of TSS is the

dominant mode, which the out-of-plane motion is small and negligible. Thus, the out-of-plane motion is not shown in the rest cases.

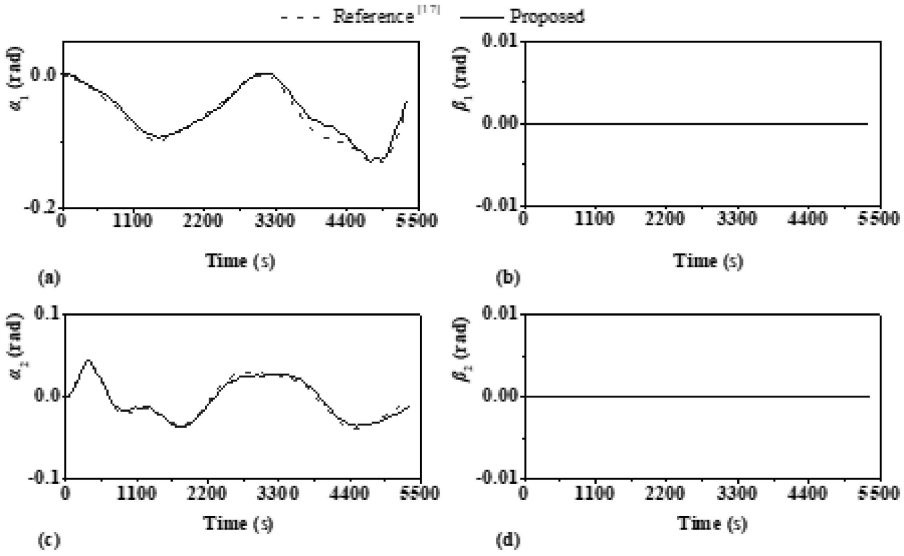

Fig. 3. Comparisons of libration angles in upward transfer. (a) Libration angle α_1. (b) Libration angle β_2.. (c) Libration angle α_2. (d) Libration angleβ_2..

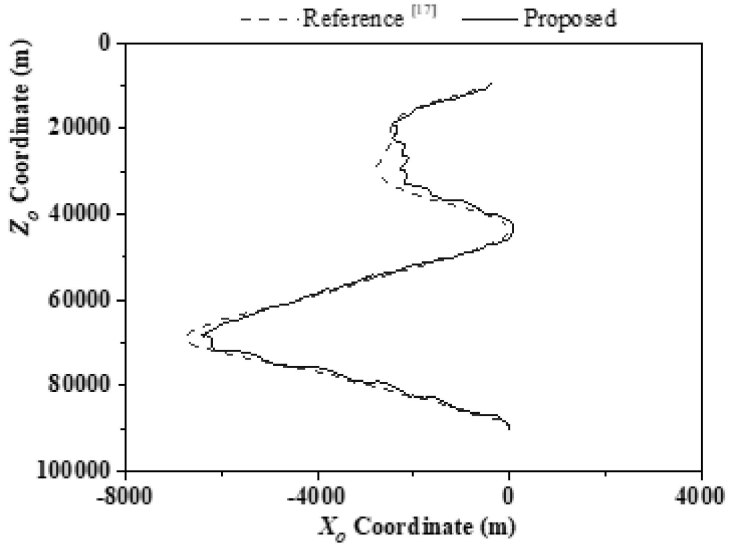

Fig. 4. Climber trajectory with respective to CM in orbital frame in upward transfer.

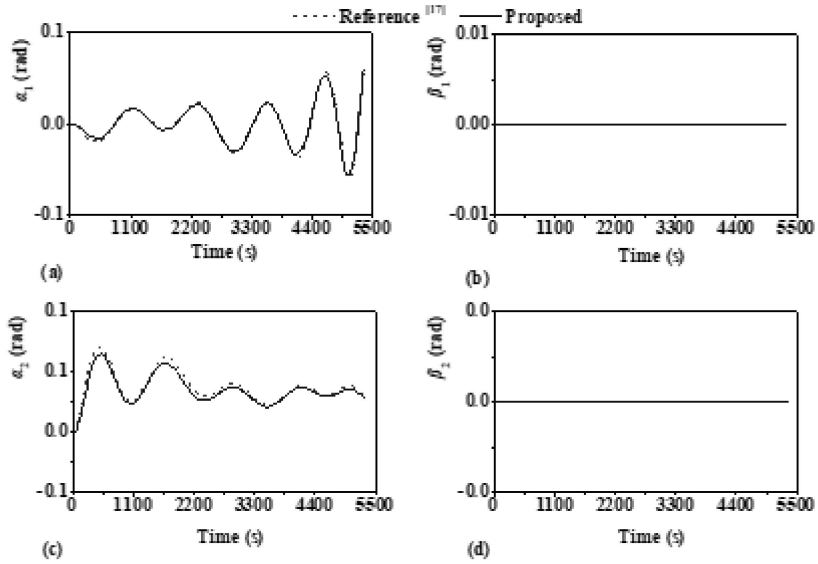

Fig. 5. Libration angles in downward transfer. (a) Libration angle α_1. (b) Libration angle β_2. (c) Libration angle α_2. (d) Libration angle β_2.

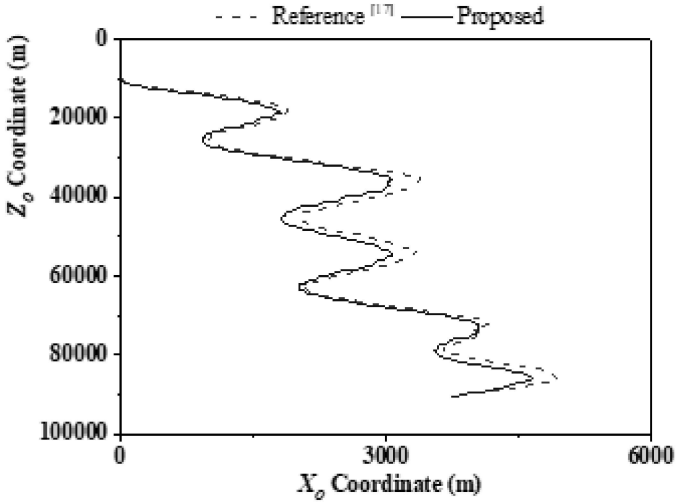

Fig. 6. Climber trajectory with respective to CM in orbital frame in downward transfer.

Moreover, the climber's movement generates transverse wave propagation along the tether. The transverse wave propagation speed along the tether is $V = \sqrt{T/\mu}$, where T is the tether tension and μ is the linear density of tether. In the design stage, an operation condition of the climber is that the velocity of climber should be much smaller than the wave propagation speed $\dot{p} < V$, where $\dot{p}$ is the velocity of climber. Taking the upward transfer as an example. Figure 7 shows the geometrical configuration of deformed tether in the first 11s. Figure 8 shows the wave

propagation from the bottom (the climber position) to the top (the main satellite). It is noted from Table 2 that the climber's speed is much smaller than the wave propagation speed. This is good because the wave propagation will not interference with the motion of climber.

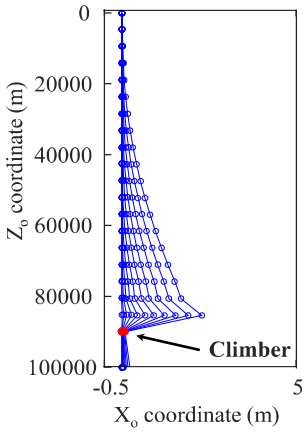

Fig. 7 Deformed tether in orbital frame in upward transfer (the first 11s in 1s interval).

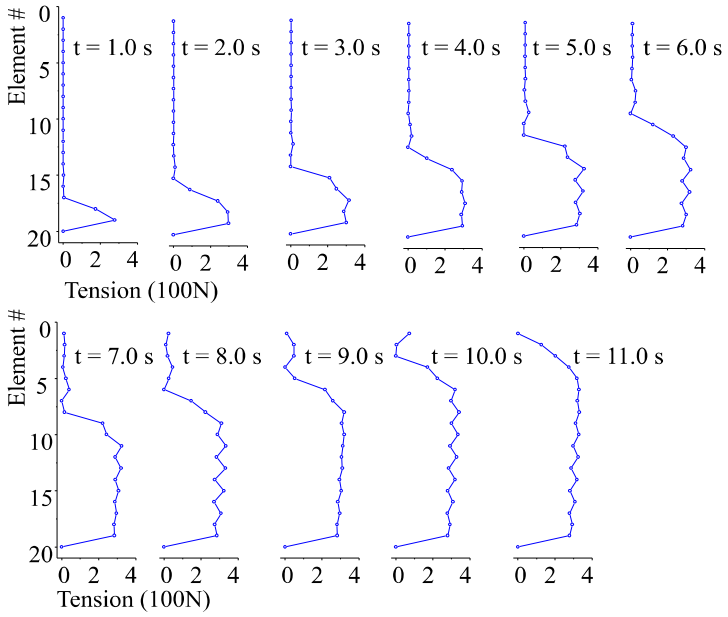

Fig. 8. Tension distribution along tether in upward transfer at different moments.

Table 2. Tether tension and corresponding wave propagation speed along the tether.

Time (s)	Tension in element connected to climber (N)	Wave propagation speed (m/s)
1	277.86	310.61
2	297.63	321.47
3	299.42	322.44
4	293.95	319.48

5	284.20	314.14
6	280.78	312.24
7	284.15	314.11
8	285.95	315.10
9	282.52	313.20
10	278.60	311.02
11	279.30	311.42

In the second validation case, the masses of the climber, the subsatellite, and the tether are no longer negligible compared with the mass of main satellite. The movement of the climber will change the CM position of the TTS system. The initial conditions and physical parameters in [5] are used: $r(0)=6600\ km$, $\psi(0)=1.178\times10^{-3}\ rad/s$, $\alpha_1(0)=\alpha_2(0)=\dot{\alpha}_1(0)=\dot{\alpha}_2(0)=0$ $L=10\ km$, $m_m=m_s=1000\ kg$, $m_c=100\ kg$, and $V=1m/s$. Only the upward movement is considered here due to the similarity exists between the upward and downward movement for this TTS. The climber starts at 100 m from the sub satellite and travels upward 9800 m along the tether. The comparisons of libration angles of the TTS and the trajectory of the climber are shown in Figs. 9-10. It can be seen that both the libration angles and trajectory agree well in general with the results of two-piece dumbbell model of [5]. However, there is noticeable differences in climber's trajectory and libration angles, see Figs. 9-10. The reason that causes the differences is the significant difference in the variation of the orbital radius of CM, see Fig. 9(a). In the current model, the CM of the TTS system is increased only by 460m as the result of upward transfer, which is the same as the simple calculation based on energy balance. Our results are also very similar to the results of Kojima et al. [17] in a similar case. The CM variation in Ref. [5] is about 30km, see Fig. 9(a). For a TTS with a 10km long tether, this implies the entire TTS is moving up and down in the upward transfer by 30km. This is unlikely because the variation of orbital potential energy is much greater than the energy input to the TTS by moving the climber upwards. To explore the influence of the orbital radius change of CM, we conducted a case study with a constant orbital

radius r = 6,600km in Eqs. (16) and (17) of Ref. [5]. The comparison is added to Fig. 9. As expected, the difference between the proposed approach and the model in Ref. [5] with a constraint r is very small. It justifies the use of Ref. [5] for validation.

In conclusion, these cases validate that the proposed method.

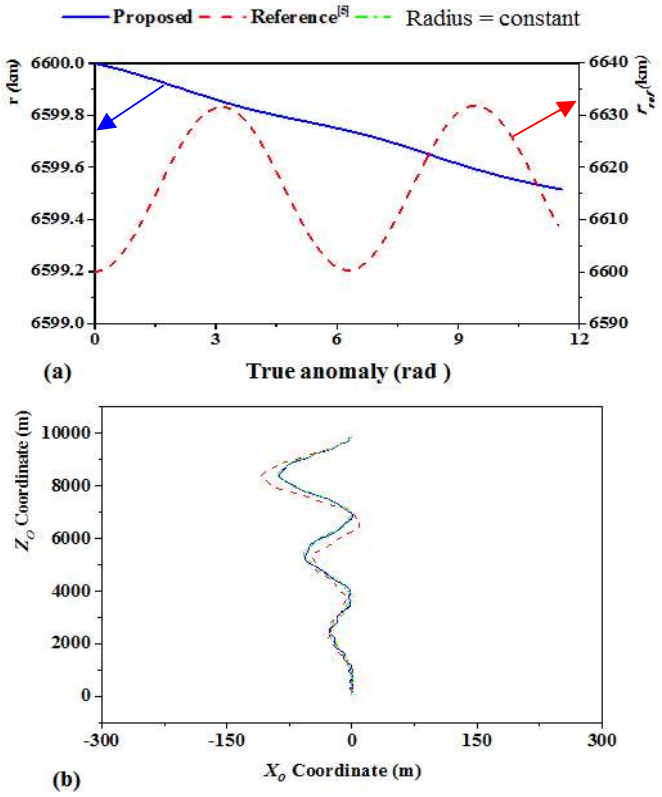

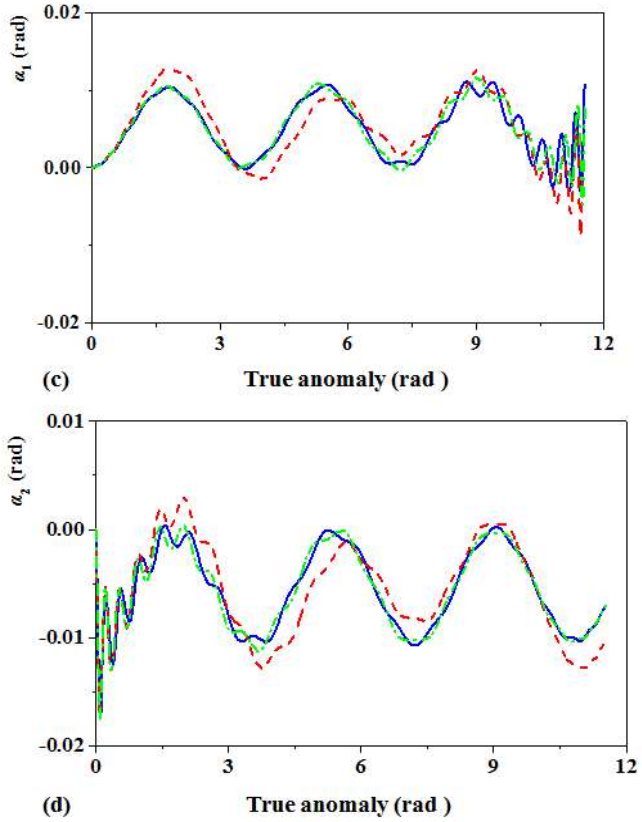

Fig. 9. Comparison results in upward transfer.

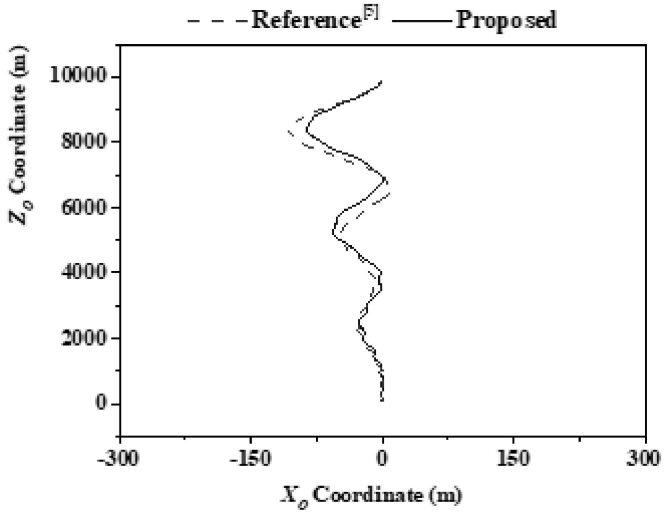

Fig. 10. Climber Trajectory with respective to CM in orbital frame in upward transfer.

B. Effect of the tether discretization scheme

In this section, the effect of the tether discretization scheme on the dynamic response of TTS with one climber is investigated. The tether was discretized into two, four, 10 elements and 20 elements,

respectively. For the number of elements greater than two, the merging and dividing elements occurs as the climber across the element boundary. Accordingly, the degree-of-freedom of the TTS model varies. The parameters of the dividing and merging elements are given as: $L_s = 3000\ m$, $L_s = 1000\ m$ and $L_s = 500\ m$ for the 4-element, the 10-element and 20-element discretization schemes respectively, $L_{max} = 1.65L_s$, $L_{\min} = 0.49L_s$, and $\delta_e = 10^{-3}\ m$. Unless noted otherwise, the following parameters of the TTS are used in this section: the circular orbital radius of CM is 6600 km, $m_m = m_s = 1000\ kg$, $m_c = 100\ kg$, $L = 10\ km$, and $V_c = 1\ m/s$. The climber starts at 0.01 L from the sub satellite and stops at 0.99L from the main satellite, which means the material coordinate of the climber changes from 100 m to 9,900 m. A converging index is defined to show the convergence of the solution of climber's position vs the element numbers,

$$R_{j,k} = \frac{\sqrt{\left(X_{c,k} - X_{c,j}\right)^2 + \left(Y_{c,k} - Y_{c,j}\right)^2 + \left(Z_{c,k} - Z_{c,j}\right)^2}}{\sqrt{X_{c,j}^2 + Y_{c,j}^2 + Z_{c,j}^2}} \times 100\%$$

where j and k represent the different successive discretization schemes.

The analysis results are shown in Figs. 11-13. It can be easily observed that the general trends of the libration angles of the TTS are similar for discretization by different element numbers, see Figs. 11-12. However, it is noted that the tether transverse oscillation motion becomes obvious with more tether elements. Therefore, it indicates that more elements should be used to capture the high frequency transverse oscillation of tether. The same phenomenon is found in the variation of tether geometrical configuration, see Fig. 13. Furthermore, the analysis also reveals that the constant velocity profile of climber is not realistic and is responsive partially for the high frequency transverse oscillation.

The influence of finite element discretization on the solution accuracy is shown in Table 3. It is noted the difference in solutions between two successive finite element discretization schemes

decreases as the element number increases. For instance, the difference between the 10-element and 20-element discretization $R_{10,20}$ is around 0.2%, which is negligible. Moreover, as the tether is discretized into more elements, the computational loads increases significantly. Therefore, the 10-element discretization is used in the following analysis.

Next, a more realistic start-stop velocity profile of the climber, instead of constant velocity, is considered to investigate the dynamic response of the TTS. The motion profile of the climber contains an acceleration phase, a constant velocity cruise phase, and a deceleration phase, as shown in Eq. (26). The non-dimensional parameter τ defines the time duration of acceleration to the time of cruise Refs. [3, 8]. In the current work, the acceleration and deceleration phases are equal:

$$p_{j,\text{desired}} = \begin{cases} -\dfrac{1}{\beta}\dfrac{L_{eq}}{\pi}\sin\left(\dfrac{1}{\tau}\pi\dfrac{V_{cr}}{L_{eq}}t\right)+\dfrac{V_{cr}}{2}t & t \le t_a \\ V_{cr}t-\dfrac{\alpha}{2}L_{eq} & t_a \le t \le t_b \\ \dfrac{1}{\beta}\dfrac{L_{eq}}{\pi}\sin\left(\dfrac{1}{\tau}\pi\dfrac{V_{cr}}{L_{eq}}\left(t-t_b\right)\right)+\dfrac{V_{cr}}{2}t+\dfrac{1-\tau}{2}L_{eq} & t_b \le t \le t_c \end{cases} \tag{26}$$

where L_{eq} and V_{cr} are the equivalent moving distance and cruise velocity, respectively. $\beta = 2/\tau$. $t_a = \tau L_{eq}/V_{cr}$, $t_b = L_{eq}/V_{cr}$, and $t_c = \left(1+\tau\right)L_{eq}/V_{cr}$.

First, the effect of the magnitude of cruise velocity on the dynamic response of TTS is investigated. The parameter α is set as 0.2, and three cases are conducted with the cruise velocity being 1 m/s, 2 m/s, and 4 m/s, respectively. The results are shown in Figs. 14 - 15. Figure 14 shows the libration angles of TTS system, where the x-axis represents the variation of material coordinate. The oscillation amplitude of the libration angles increases as the magnitude of cruise velocity increases. The same phenomenon can be observed from the trajectories of two satellites and the climber, seen Fig. 15.

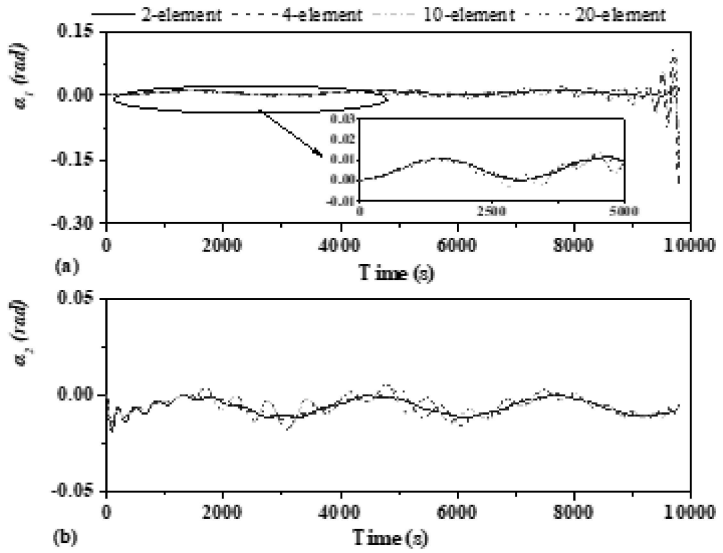

Fig. 11. Libration angles in the upward transfer motion (a) α_1 and (b) α_2

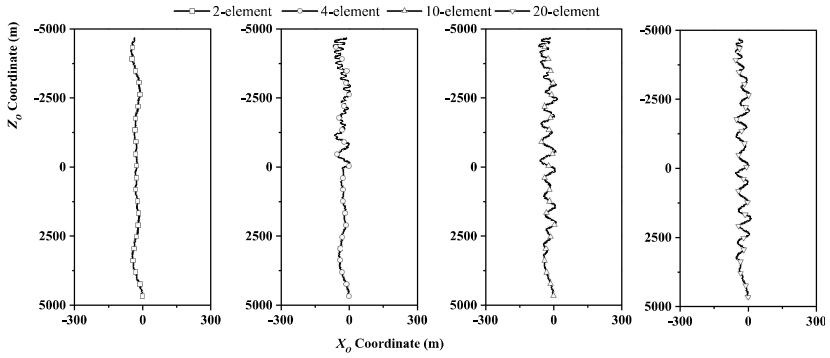

Fig. 12. Trajectory of the climber in the orbital frame by different discretization schemes.

Table 3. Convergence of position solution of climber vs different discretization schemes

Time (s)	$R_{2,4}$ (%)	$R_{4,10}$ (%)	$R_{10,20}$ (%)
100	2.71	0.51	0.18
2000	7.78	0.90	0.03
4000	2.93	0.96	0.20
6000	1.12	0.69	0.21
8000	9.18	0.29	0.12
9500	2.87	0.54	0.23

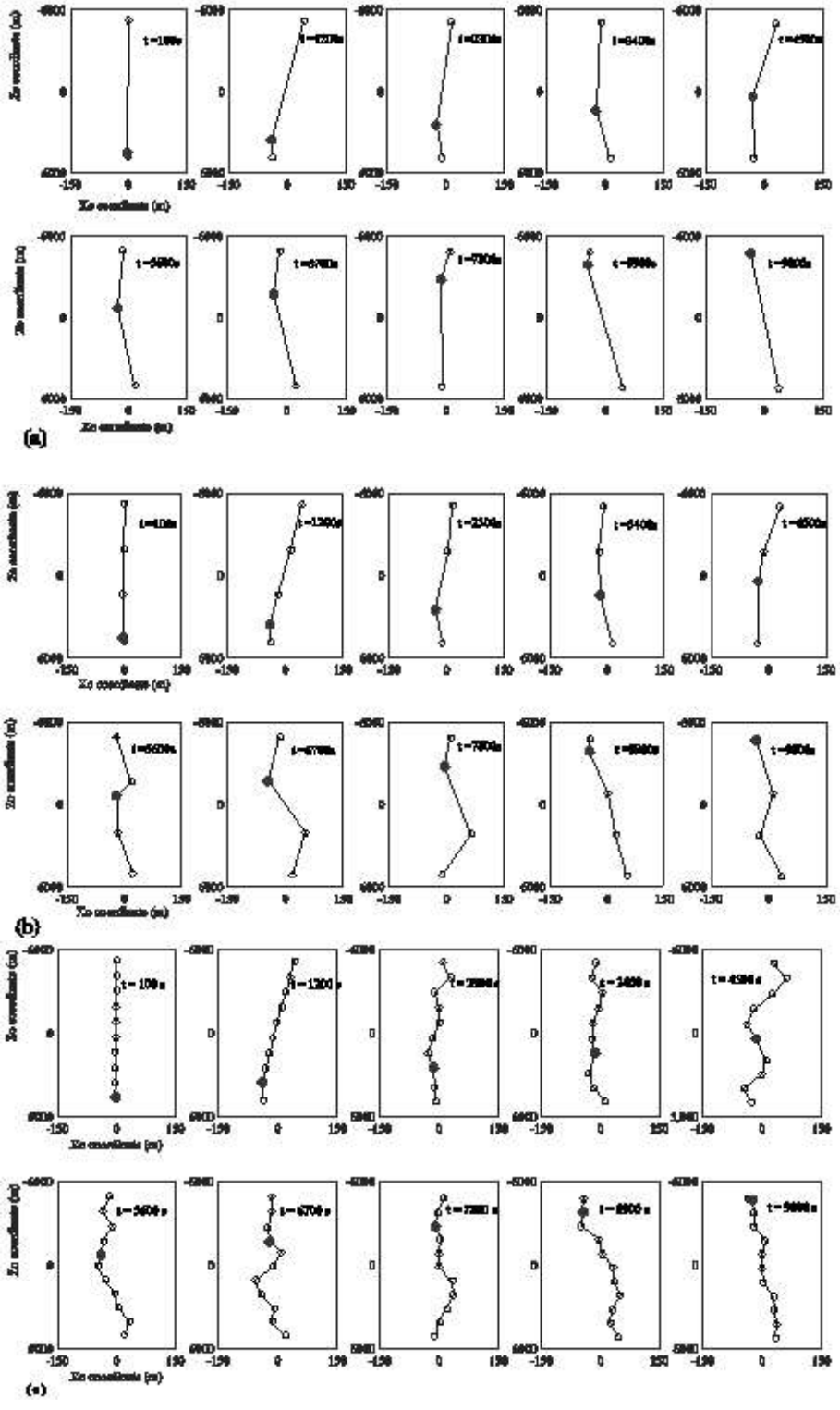

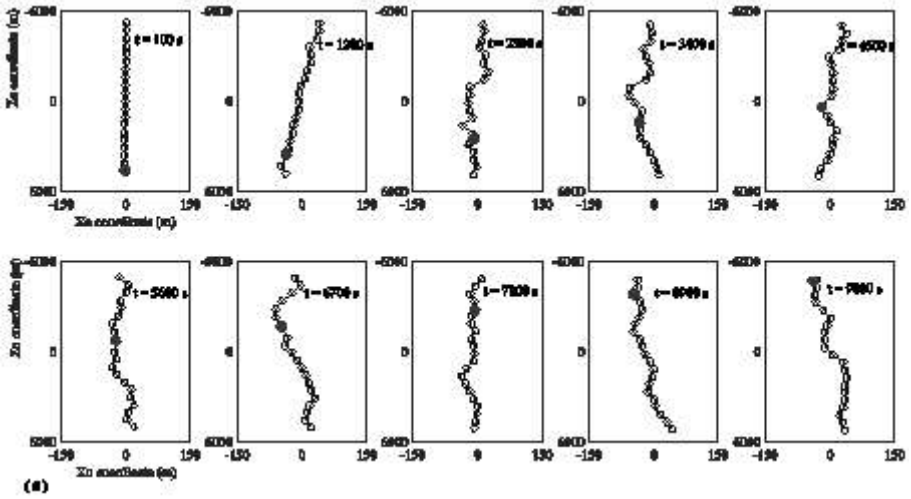

Fig. 13. Calculated configuration of TTS with (a) 2-element. (b) 4-elements (c) 10-elements (d) 20-elements.

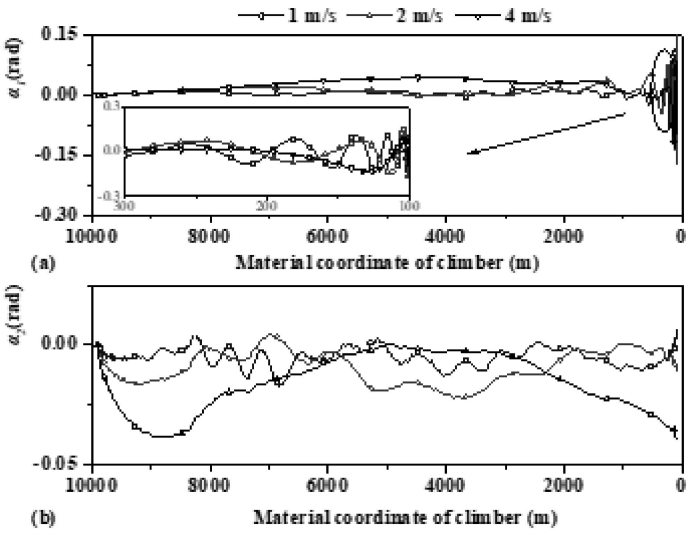

Fig. 14. Libration angles (a) α_1 and (b) α_2 corresponding to different cruise velocities.

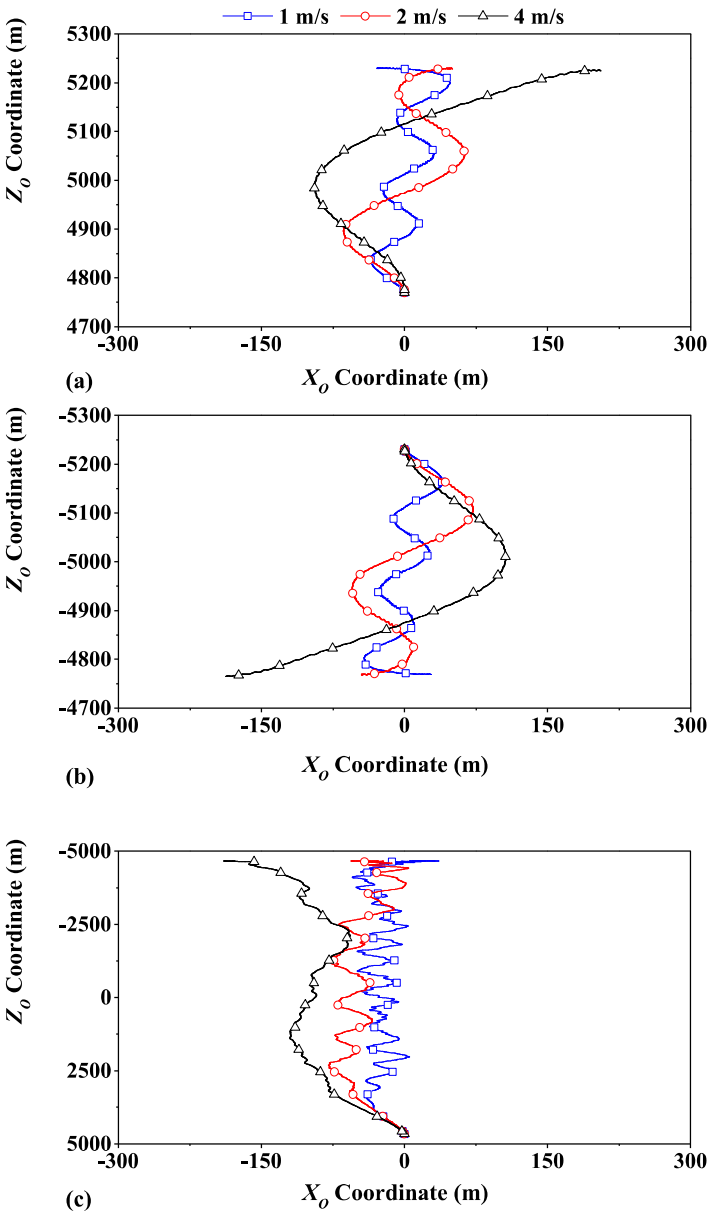

Fig. 15. Trajectories in the orbital frame: (a) main satellite (b) sub satellite (c) climber.

Then, the effect of parameter α on the dynamic response of TTS system is investigated. The cruise velocity V_{cr} is set as 4 m/s. Four cases are conducted with α being 0.1, 0.3, 0.6, and 0.9, respectively. As show in Fig. 16, the total time of the transient motion varies due to different values of α. To observe the residual libration of the climber upon climber arrest, the simulation time is extended by 1,000 s. The results are shown in Fig. 17. It shows the α significantly affects the libration angles. The increase of α represents the decrease of the applied Coriolis force induced by

the climber motion. Furthermore, the residual libration motion is observed and the amplitude of residual libration decreases as the time α increases. The results indicate that gradual acceleration and deceleration is helpful for the suppression of libration angles of the climber.

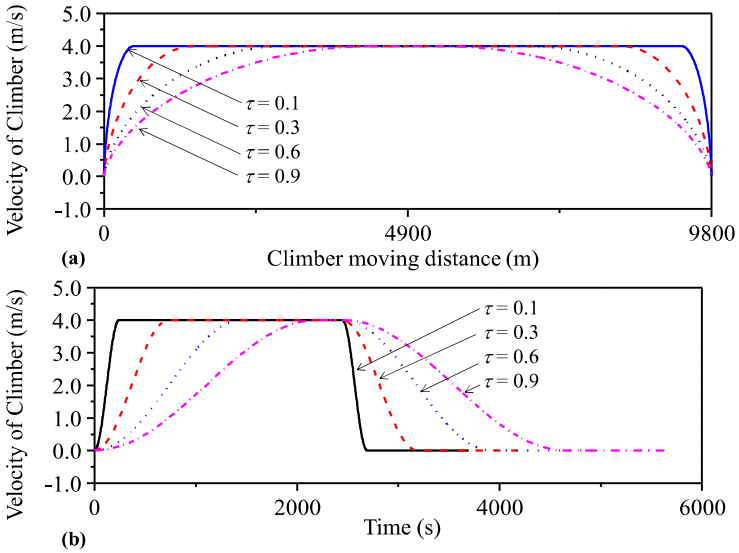

Fig. 16. Velocity profiles of climber with different values of τ.

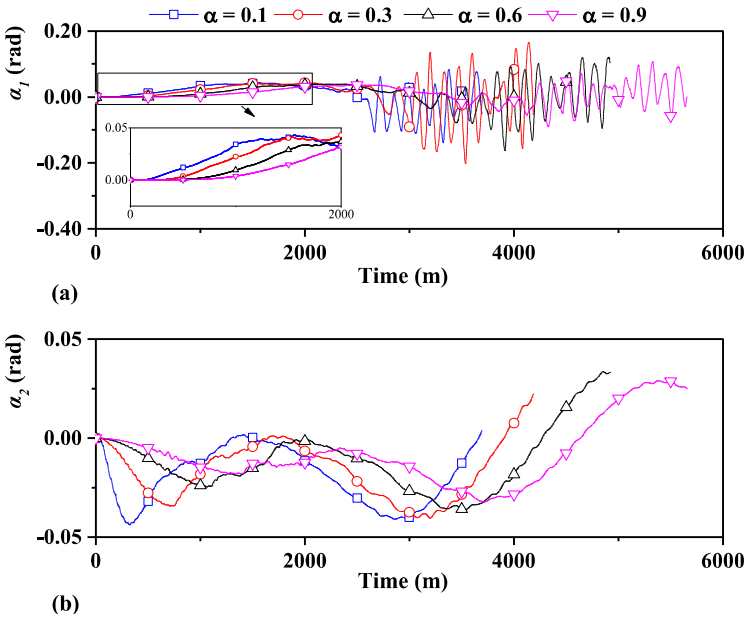

Fig. 17. Libration angles: (a) Libration angle α_1. (b) Libration angle α_2.

C. The dynamic behavior of TTS with multiple climbers

Multiple climbers with proper phase shift have been proposed to suppress the libration of TTS

down to zero [2, 3]. For simplicity, each climber is assumed to be the same (same mass = 33.333kg) and to move with the same velocity profile in Eq. (26). Each one is launched with a delay of 100 s. The parameter α is 0.2, the cruise velocity V_{cr} is 4 m/s and the equivalent moving length L_{eq} is 9,867 m. As shown in Fig. 18, both the upward and downward transfers of climbers are analyzed. The results are shown in Figs. 19-21.

The time history of libration angles is shown in Fig. 19. It is easily seen that the libration angles experience a high frequency oscillation as the climbers approaching to the end. This is because the climbers are too closer to each other at the end, and the shorter the tether between the climbers the higher the oscillation frequency. Figure 20 shows the variation of the main and sub satellite positions in the orbital frame. It can be found that both satellites move in the Z-axis of the orbital frame, seen in Fig. 20(a) and (c). The reason for this phenomenon is that the CM of the TTS changes as the climber moves up/down, and the origin of the orbital frame is at the CM position. For example, both the main and sub satellites move up for the upward transfer motion by 459m and 467m, respectively. These two values are a slightly different from analytical solutions of 463m, which is calculated based on the rigid vertical tether model. The difference is caused by the swing libration motion of the TTS and the bending of tether; see Fig. 20(b) and (d) and Fig. 21, which is ignored in the analytical solution.

In conclusion, the proposed method reveals the high frequency oscillation of TTS in the orbital transfer, which is not available by the rigid tether model. The oscillation could affect adversely the safe operation of TTS, especially causing the fatigue failure of tether, and must be considered.

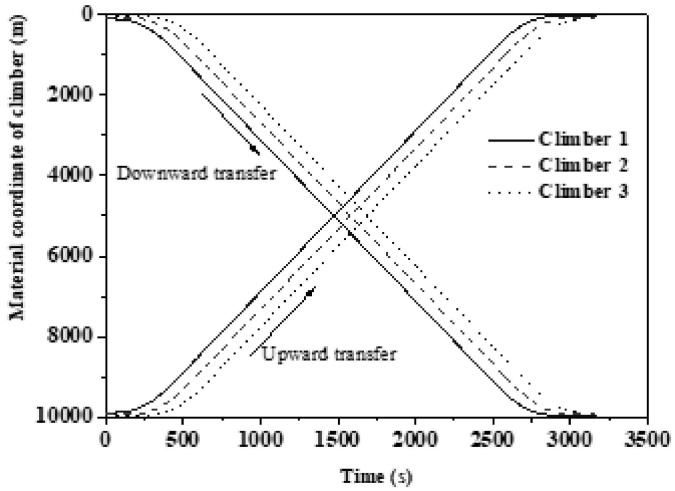

Fig. 18. Climber movement with a phase shift in the upward and downward transfer cases.

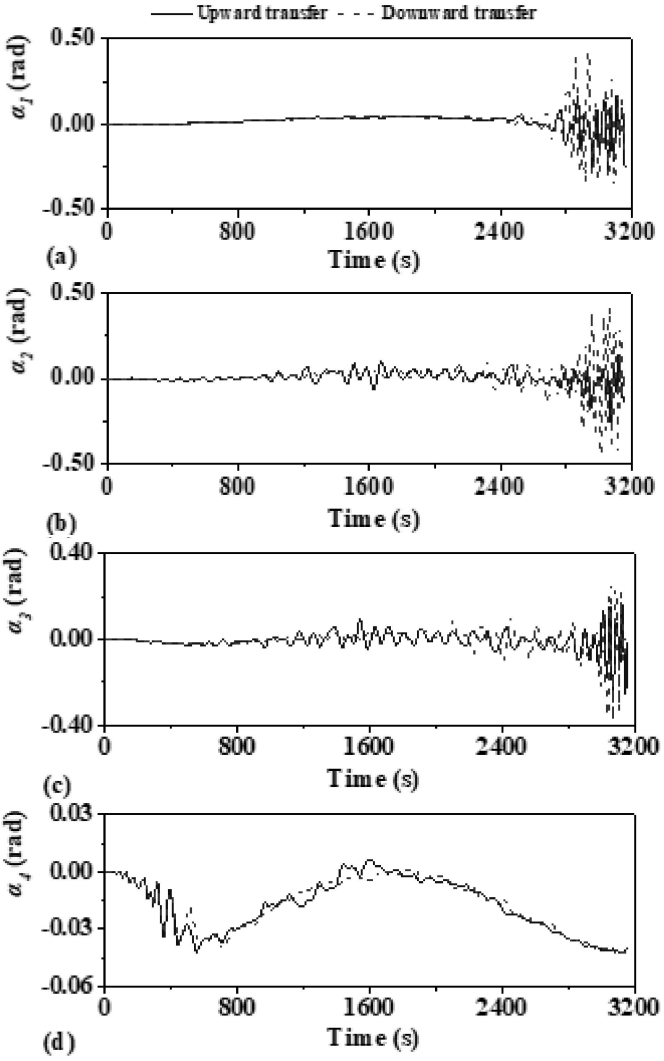

Fig. 19. Libration angles with three climbers in the upward and downward transfer cases.

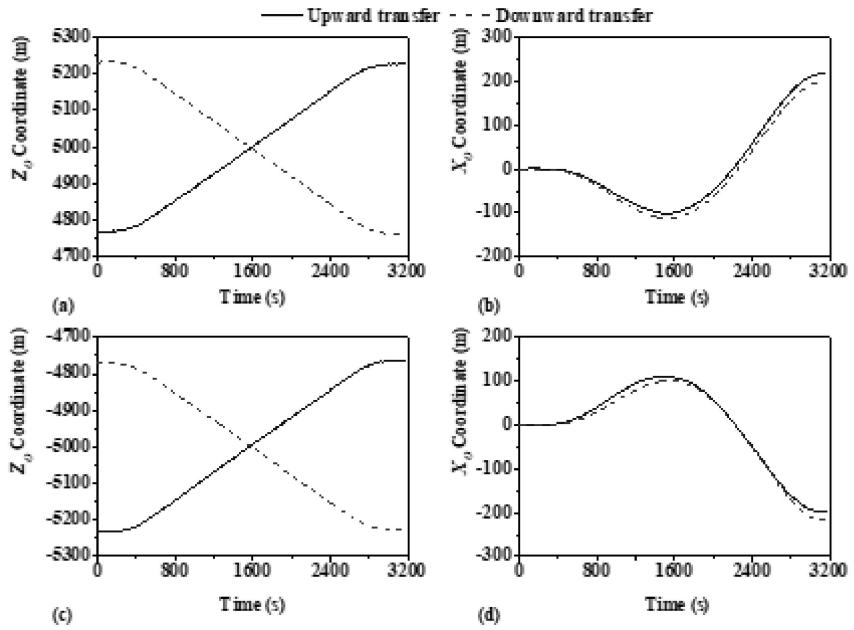

Fig. 20. Displacements of the main and sub satellites.

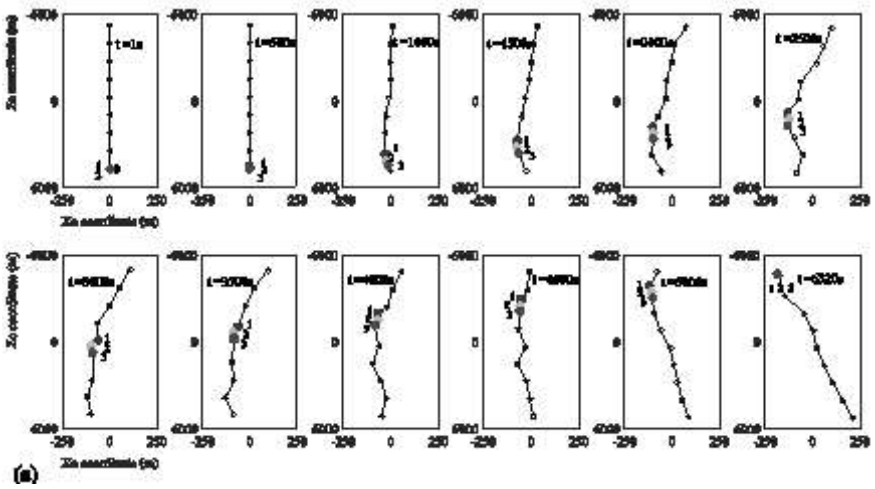

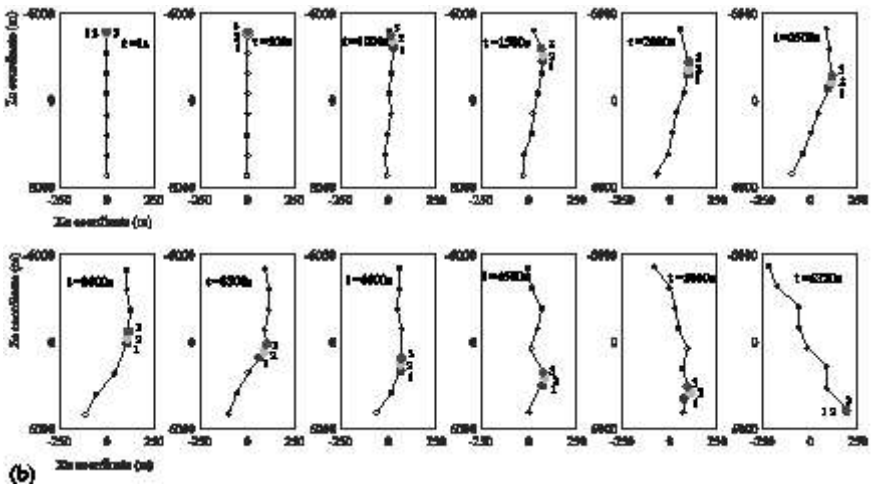

Fig. 21. Tether geometry in the orbital frame (a) upward transfer (b) downward transfer.

IV. Conclusions

A high-fidelity model of the tether transportation system is proposed by the nodal position finite element in the arbitrary Lagrangian-Eulerian description. A material coordinate is introduced as the state variable that is not associated with the finite element mesh. Two types of element are defined, the variable-length and constant-length elements, and the nodes where the climbers located are defined as the moving nodes associated with the material coordinates. The proposed method reveals that the orbital transfer by the climber will induce high frequency transfer oscillation of tether, which is not discovered by the existing rigid tether approach. The oscillation could lead to the fatigue failure of tether and must be considered.

Acknowledgements

This work is supported by the Discovery Grant (No. 2018-05991) of Natural Sciences and Engineering Research Council of Canada and the FAST grant of Canadian Space Agency.

Appendix

A. The extended mass matrix $\boldsymbol{M}_{e,k}$ can be written as,

$$\boldsymbol{M}_{e,k}=\begin{pmatrix}\boldsymbol{M}_{11} & \boldsymbol{M}_{12} & \boldsymbol{M}_{13}\\ \boldsymbol{M}_{12}^{T} & \boldsymbol{M}_{22} & \boldsymbol{M}_{23}\\ \boldsymbol{M}_{12}^{T} & \boldsymbol{M}_{23}^{T} & \boldsymbol{M}_{33}\end{pmatrix} \tag{A.1}$$

where the sub matrix $\boldsymbol{M}_{11}$ is the same as Refs. [18, 19], the others are defined as follows,

$$\boldsymbol{M}_{12}=\left(\frac{p_{k+1}-p_k}{2}\right)\int_{-1}^{1}\rho_k A_k \boldsymbol{N}_{a,k}^{T}\frac{\partial \boldsymbol{N}_{a,k}}{\partial p_k}d\xi \boldsymbol{X}_{a,k} \tag{A.2}$$

$$\boldsymbol{M}_{13}=\left(\frac{p_{k+1}-p_k}{2}\right)\int_{-1}^{1}\rho_k A_k \boldsymbol{N}_{a,k}^{T}\frac{\partial \boldsymbol{N}_{a,k}}{\partial p_{k+1}}d\xi \boldsymbol{X}_{a,k} \tag{A.3}$$

$$\boldsymbol{M}_{22}=\boldsymbol{X}_{a,k}^{T}\left(\frac{p_{k+1}-p_k}{2}\right)\int_{-1}^{1}\rho_k A_k \left(\frac{\partial \boldsymbol{N}_{a,k}}{\partial p_k}\right)^{T}\frac{\partial \boldsymbol{N}_{a,k}}{\partial p_k}d\xi \boldsymbol{X}_{a,k} \tag{A.4}$$

$$\boldsymbol{M}_{23}=\boldsymbol{X}_{a,k}^{T}\left(\frac{p_{k+1}-p_k}{2}\right)\int_{-1}^{1}\rho_k A_k \left(\frac{\partial \boldsymbol{N}_{a,k}}{\partial p_k}\right)^{T}\frac{\partial \boldsymbol{N}_{a,k}}{\partial p_{k+1}}d\xi \boldsymbol{X}_{a,k} \tag{A.5}$$

$$\boldsymbol{M}_{33}=\boldsymbol{X}_{a,k}^{T}\left(\frac{p_{k+1}-p_k}{2}\right)\int_{-1}^{1}\rho_k A_k \left(\frac{\partial \boldsymbol{N}_{a,k}}{\partial p_{k+1}}\right)^{T}\frac{\partial \boldsymbol{N}_{a,k}}{\partial p_{k+1}}d\xi \boldsymbol{X}_{a,k} \tag{A.6}$$

B. The detailed expressions of the additional term $\boldsymbol{Q}_{p,k}$ due to the mass flow are obtained as,

$$\boldsymbol{Q}_{p,k}=\sum_{j=1}^{5}\boldsymbol{Q}_{p,k}^{j} \tag{B.1}$$

$$\boldsymbol{Q}_{p,k}^{1}=\begin{bmatrix}\boldsymbol{Q}_{p,k}^{1,1} & \boldsymbol{Q}_{p,k}^{1,2} & \boldsymbol{Q}_{p,k}^{1,3}\end{bmatrix} \tag{B.2}$$

$$\boldsymbol{Q}_{p,k}^{1,1}=\rho_k A_k\left(p_{k+1}-p_k\right)\dot{p}_k\int_{-1}^{1}\boldsymbol{N}_{a,k}^{T}\frac{\partial \boldsymbol{N}_{a,k}}{\partial p_k}d\xi \dot{\boldsymbol{X}}_{a,k} \tag{B.3}$$

$$\boldsymbol{Q}_{p,k}^{1,2}=\rho_k A_k\left(p_{k+1}-p_k\right)\dot{p}_k \boldsymbol{X}_{a,k}^{T}\int_{-1}^{1}\left(\frac{\partial \boldsymbol{N}_{a,k}}{\partial p_k}\right)^{T}\frac{\partial \boldsymbol{N}_{a,k}}{\partial p_k}d\xi \dot{\boldsymbol{X}}_{a,k} \tag{B.4}$$

$$\boldsymbol{Q}_{p,k}^{1,3}=\rho_k A_k\left(p_{k+1}-p_k\right)\dot{p}_k \boldsymbol{X}_{a,k}^{T}\int_{-1}^{1}\left(\frac{\partial \boldsymbol{N}_{a,k}}{\partial p_{k+1}}\right)^{T}\frac{\partial \boldsymbol{N}_{a}}{\partial p_k}d\xi \dot{\boldsymbol{X}}_{a,k} \tag{B.5}$$

$$\boldsymbol{Q}_{p,k}^{2}=\begin{bmatrix}\boldsymbol{Q}_{p,k}^{2,1} & \boldsymbol{Q}_{p,k}^{2,2} & \boldsymbol{Q}_{p,k}^{2,3}\end{bmatrix} \tag{B.6}$$

$$\boldsymbol{Q}_{p,k}^{2,1}=\rho_k A_k\left(p_{k+1}-p_k\right)\dot{p}_{k+1}\int_{-1}^{1}\boldsymbol{N}_{a,k}^{T}\frac{\partial \boldsymbol{N}_{a,k}}{\partial p_{k+1}}d\xi\dot{\boldsymbol{X}}_{a,k} \tag{B.7}$$

$$\boldsymbol{Q}_{p,k}^{2,2}=\rho_k A_k\left(p_{k+1}-p_k\right)\dot{p}_{k+1}\boldsymbol{X}_{a,k}^{T}\int_{-1}^{1}\left(\frac{\partial \boldsymbol{N}_{a,k}}{\partial p_k}\right)^{T}\frac{\partial \boldsymbol{N}_{a,k}}{\partial p_{k+1}}d\xi\dot{\boldsymbol{X}}_{a,k} \tag{B.8}$$

$$\boldsymbol{Q}_{p,k}^{1,3}=\rho_k A_k\left(p_{k+1}-p_k\right)\dot{p}_{k+1}\boldsymbol{X}_{a,k}^{T}\int_{-1}^{1}\left(\frac{\partial \boldsymbol{N}_{a,k}}{\partial p_{k+1}}\right)^{T}\frac{\partial \boldsymbol{N}_{a}}{\partial p_{k+1}}d\xi\dot{\boldsymbol{X}}_{a,k} \tag{B.9}$$

$$\boldsymbol{Q}_{p,k}^{3}=\begin{bmatrix}\boldsymbol{Q}_{p,k}^{3,1} & \boldsymbol{Q}_{p,k}^{3,2} & \boldsymbol{Q}_{p,k}^{3,3}\end{bmatrix} \tag{B.10}$$

$$\boldsymbol{Q}_{p,k}^{3,1}=\rho_k A_k\left(\frac{p_{k+1}-p_k}{2}\right)\dot{p}_k^{2}\int_{-1}^{1}\boldsymbol{N}_{a,k}^{T}\frac{\partial^2 \boldsymbol{N}_{a,k}}{\partial p_k^{2}}d\xi\boldsymbol{X}_{a,k} \tag{B.11}$$

$$\boldsymbol{Q}_{p,k}^{3,2}=\rho_k A_k\left(\frac{p_{k+1}-p_k}{2}\right)\dot{p}_k^{2}\boldsymbol{X}_{a,k}^{T}\int_{-1}^{1}\left(\frac{\partial \boldsymbol{N}_{a,k}}{\partial p_k}\right)^{T}\frac{\partial^2 \boldsymbol{N}_{a,k}}{\partial p_k^{2}}d\xi\boldsymbol{X}_{a,k} \tag{B.12}$$

$$\boldsymbol{Q}_{p,k}^{3,3}=\rho_k A_k\left(\frac{p_{k+1}-p_k}{2}\right)\dot{p}_k^{2}\boldsymbol{X}_{a,k}^{T}\int_{-1}^{1}\left(\frac{\partial \boldsymbol{N}_{a,k}}{\partial p_{k+1}}\right)^{T}\frac{\partial^2 \boldsymbol{N}_{a,k}}{\partial p_k^{2}}d\xi\boldsymbol{X}_{a,k} \tag{B.13}$$

$$\boldsymbol{Q}_{p,k}^{4}=\begin{bmatrix}\boldsymbol{Q}_{p,k}^{4,1} & \boldsymbol{Q}_{p,k}^{4,2} & \boldsymbol{Q}_{p,k}^{4,3}\end{bmatrix} \tag{B.14}$$

$$\boldsymbol{Q}_{p,k}^{4,1}=\rho_k A_k\left(\frac{p_{k+1}-p_k}{2}\right)\dot{p}_{k+1}^{2}\int_{-1}^{1}\boldsymbol{N}_{a,k}^{T}\frac{\partial^2 \boldsymbol{N}_{a,k}}{\partial p_{k+1}^{2}}d\xi\boldsymbol{X}_{a,k} \tag{B.15}$$

$$\boldsymbol{Q}_{p,k}^{4,2}=\rho_k A_k\left(\frac{p_{k+1}-p_k}{2}\right)\dot{p}_{k+1}^{2}\boldsymbol{X}_{a,k}^{T}\int_{-1}^{1}\left(\frac{\partial \boldsymbol{N}_{a,k}}{\partial p_k}\right)^{T}\frac{\partial^2 \boldsymbol{N}_{a,k}}{\partial p_{k+1}^{2}}d\xi\boldsymbol{X}_{a,k} \tag{B.16}$$

$$\boldsymbol{Q}_{p,k}^{4,3}=\rho_k A_k\left(\frac{p_{k+1}-p_k}{2}\right)\dot{p}_{k+1}^{2}\boldsymbol{X}_{a,k}^{T}\int_{-1}^{1}\left(\frac{\partial \boldsymbol{N}_{a,k}}{\partial p_{k+1}}\right)^{T}\frac{\partial^2 \boldsymbol{N}_{a,k}}{\partial p_{k+1}^{2}}d\xi\boldsymbol{X}_{a,k} \tag{B.17}$$

$$\boldsymbol{Q}_{p,k}^{5}=\begin{bmatrix}\boldsymbol{Q}_{p,k}^{5,1} & \boldsymbol{Q}_{p,k}^{5,2} & \boldsymbol{Q}_{p,k}^{5,3}\end{bmatrix} \tag{B.18}$$

$$\boldsymbol{Q}_{p,k}^{5,1}=\rho_k A_k\left(\frac{p_{k+1}-p_k}{2}\right)\dot{p}_k\dot{p}_{k+1}\int_{-1}^{1}\boldsymbol{N}_{a,k}^{T}\frac{\partial^2\boldsymbol{N}_{a,k}}{\partial p_k\partial p_{k+1}}d\xi\boldsymbol{X}_{a,k} \tag{B.19}$$

$$\boldsymbol{Q}_{p,k}^{5,2}=\rho_k A_k\left(\frac{p_{k+1}-p_k}{2}\right)\dot{p}_k\dot{p}_{k+1}\boldsymbol{X}_{a,k}^{T}\int_{-1}^{1}\left(\frac{\partial\boldsymbol{N}_{a,k}}{\partial p_k}\right)^{T}\frac{\partial^2\boldsymbol{N}_{a,k}}{\partial p_k\partial p_{k+1}}d\xi\boldsymbol{X}_{a,k} \tag{B.20}$$

$$\boldsymbol{Q}_{p,k}^{5,3}=\rho_k A_k\left(\frac{p_{k+1}-p_k}{2}\right)\dot{p}_k\dot{p}_{k+1}\boldsymbol{X}_{a,k}^{T}\int_{-1}^{1}\left(\frac{\partial\boldsymbol{N}_{a,k}}{\partial p_{k+1}}\right)^{T}\frac{\partial^2\boldsymbol{N}_{a,k}}{\partial p_k\partial p_{k+1}}d\xi\boldsymbol{X}_{a,k} \tag{B.21}$$

C. The detailed expressions of elastic force $\boldsymbol{Q}_{e,k}=\left(\boldsymbol{Q}_{e,k}^{1},\boldsymbol{Q}_{e,k}^{2},\boldsymbol{Q}_{e,k}^{3}\right)^{T}$ are as,

$$\boldsymbol{Q}_{e,k}^{1}=-\left(\frac{2}{p_{k+1}-p_k}\right)\bar{\varepsilon}_{0,k}E_k A_k\int_{-1}^{1}\left(\frac{\partial\boldsymbol{N}_{a,k}}{\partial\xi}\right)^{T}\left(\frac{\partial\boldsymbol{N}_{a,k}}{\partial\xi}\right)d\xi\boldsymbol{X}_{a,k} \tag{C.1}$$

$$\boldsymbol{Q}_{e,k}^{2}=\frac{1}{\left(p_{k+1}-p_k\right)^2}\bar{\varepsilon}_{0,k}E_k A_k\boldsymbol{X}_{a,k}^{T}\int_{-1}^{1}\left(\frac{\partial\boldsymbol{N}_{a,k}}{\partial\xi}\right)^{T}\left(\frac{\partial\boldsymbol{N}_{a,k}}{\partial\xi}\right)d\xi\boldsymbol{X}_{a,k} \tag{C.2}$$

$$\boldsymbol{Q}_{e,k}^{3}=-\frac{1}{\left(p_{k+1}-p_k\right)^2}\bar{\varepsilon}_{0,k}E_k A_k\boldsymbol{X}_{a,k}^{T}\int_{-1}^{1}\left(\frac{\partial\boldsymbol{N}_{a,k}}{\partial\xi}\right)^{T}\left(\frac{\partial\boldsymbol{N}_{a,k}}{\partial\xi}\right)d\xi\boldsymbol{X}_{a,k} \tag{C.3}$$

where $\bar{\varepsilon}_{0,k}$ is the average value of strain in the *k-th* element.

The detailed expressions of the gravitational force term $\boldsymbol{Q}_{g,k}=\left(\boldsymbol{Q}_{g,k}^{1},\boldsymbol{Q}_{g,k}^{2},\boldsymbol{Q}_{g,k}^{3}\right)^{T}$ are,

$$\boldsymbol{Q}_{g,k}^{1}=\left(\frac{p_{k+1}-p_k}{2}\right)\int_{-1}^{1}\boldsymbol{N}_{a,k}^{T}\boldsymbol{f}_{g,k}d\xi \tag{D.1}$$

$$\boldsymbol{Q}_{g,k}^{2}=\boldsymbol{X}_{a,k}^{T}\left(\frac{p_{k+1}-p_k}{2}\right)\int_{-1}^{1}\left(\frac{\partial\boldsymbol{N}_{a,k}}{\partial p_k}\right)^{T}d\xi\boldsymbol{f}_{g,k} \tag{D.2}$$

$$\boldsymbol{Q}_{g,k}^{3}=\boldsymbol{X}_{a,k}^{T}\left(\frac{p_{k+1}-p_k}{2}\right)\int_{-1}^{1}\left(\frac{\partial\boldsymbol{N}_{a,k}}{\partial p_{k+1}}\right)^{T}d\xi\boldsymbol{f}_{g,k} \tag{D.3}$$

References

[1] Woo P., Misra A.K., "Energy considerations in the partial space elevator," *Acta Astronautica*,

Vol. 99, No. 2014, pp.78-84.
doi: 10.1016/j.actaastro.2014.02.013.

[2] Woo P., Misra A.K., "Dynamics of a partial space elevator with multiple climbers," *Acta Astronautica*, Vol. 67, No. 7, 2010, pp.753-763.
doi: 10.1016/j.actaastro.2010.04.023.

[3] Cohen S.S., Misra A.K., "The effect of climber transit on the space elevator dynamics," *Acta Astronautica*, Vol. 64, No. 5, 2009, pp.538-553.
doi: 10.1016/j.actaastro.2008.10.003.

[4] Shi G., Zhu Z., Zhu Z.H., "Libration suppression of tethered space system with a moving climber in circular orbit," *Nonlinear Dynamics*, Vol. 91, No. 2, 2018, pp.923-937.
doi: 10.1007/s11071-017-3919-x.

[5] Jung W., Mazzoleni A.P., Chung J., "Dynamic analysis of a tethered satellite system with a moving mass," *Nonlinear Dynamics*, Vol. 75, No. 1, 2014, pp.267-281.
doi: 10.1007/s11071-013-1064-8.

[6] Cohen S.S., Misra A.K., "Elastic Oscillations of the Space Elevator Ribbon," *Journal of Guidance, Control, and Dynamics*, Vol. 30, No. 6, 2007, pp.1711-1717.
doi: 10.2514/1.29010.

[7] Williams P., "Dynamic multibody modeling for tethered space elevators," *Acta Astronautica*, Vol. 65, No. 3, 2009, pp.399-422.
doi: /10.1016/j.actaastro.2008.11.016.

[8] Sun X., Xu M., Zhong R., "Dynamic analysis of the tether transportation system using absolute nodal coordinate formulation," *Acta Astronautica*, Vol.139, October. 2017, pp.266-277.
doi: 0.1016/j.actaastro.2017.07.020.

[9] Ishikawa Y., Otsuka K., Yamagiwa Y., Doi H., "Effects of ascending and descending climbers

on space elevator cable dynamics," *Acta Astronautica*, Vol.145, April. 2018, pp.165-173.
doi: 10.1016/j.actaastro.2018.01.031.

[10] Fujii H.A., Watanabe T., Kusagaya T., Sato D., Ohta M., "Dynamics of a Flexible Space Tether Equipped with a Crawler Mass," *Journal of Guidance, Control, and Dynamics*, Vol. 31, No. 2, 2008, pp.436-440.
doi: 10.2514/1.26240.

[11] Tao K., Yamagiwa Y., Otsuka K., Ishikawa Y., "Study about the simultaneous deployment performance of the cables from GEO station at the space elevator construction," *Acta Astronautica*, Vol. 138, No. 2017, pp.590-595.
doi: 10.1016/j.actaastro.2017.01.032.

[12] Aslanov V.S., Ledkov A.S., Misra A.K., Guerman A.D., "Dynamics of Space Elevator After Tether Rupture," *Journal of Guidance, Control, and Dynamics*, Vol. 36, No. 4, 2013, pp.986-992.
doi: 10.2514/1.59378.

[13] Zanutto D., Lorenzini E.C., Mantellato R., Colombatti G., Sánchez Torres A., "Orbital debris mitigation through deorbiting with passive electrodynamic drag," *63th International Astronautical Congress*, The International Astronautical Federation IAC-12-D9.2.8, Naples, Italy, 2012.

[14] Yu B.S., Dai P.B., Jin D.P., "Modeling and dynamics of a bare tape-shaped tethered satellite system," *Aerospace Science and Technology*, Vol.79,August, 2018, pp.288-296.
doi: 10.1016/j.ast.2018.05.046.

[15] Aslanov V.S., Ledkov A.S., "Dynamics of Reusable Tether System with Sliding Bead Capsule for Deorbiting Small Payloads," *Journal of Spacecraft and Rockets*, Vol. 55, No. 6, 2018, pp. 1519-1527.
doi: 10.2514/1.A34202.

[16] Wen H., Zhu Z.H., Jin D., Hu H., "Space Tether Deployment Control with Explicit Tension Constraint and Saturation Function," *Journal of Guidance, Control, and Dynamics*, Vol. 39, No. 4, 2015, pp.916-921.
doi: 10.2514/1.G001356.

[17] Kojima H., Sugimoto Y., Furukawa Y., "Experimental study on dynamics and control of tethered satellite systems with climber," *Acta Astronautica*, Vol. 69, No. 1, 2011, pp.96-108.
doi: 10.1016/j.actaastro.2011.02.009.

[18] Sun F.J., Zhu Z.H., LaRosa M., "Dynamic modeling of cable towed body using nodal position finite element method," *Ocean Engineering*, Vol. 38, No. 4, 2011, pp.529-540.
doi: 10.1016/j.oceaneng.2010.11.016.

[19] Li G.Q., Zhu Z.H., "Long-term dynamic modeling of tethered spacecraft using nodal position finite element method and symplectic integration," *Celestial Mechanics and Dynamical Astronomy*, Vol. 123, No. 4, 2015, pp.363-386.
doi: 10.1007/s10569-015-9640-5.

[20] Zhu Z.H., "Dynamic modeling of cable system using a new nodal position finite element method," *International Journal for Numerical Methods in Biomedical Engineering*, Vol. 26, No. 6, 2010, pp.692-704.
doi: doi:10.1002/cnm.1161.

[21] Li G., Zhu Z.H., Cain J., Newland F., Czekanski A., "Libration Control of Bare Electrodynamic Tethers Considering Elastic–Thermal–Electrical Coupling," *Journal of Guidance, Control, and Dynamics*, Vol. 39, No. 3, 2015, pp.642-654.
doi: 10.2514/1.G001338.

[22] Li G., Zhu Z.H., Ruel S., Meguid S.A., "Multiphysics elastodynamic finite element analysis of space debris deorbit stability and efficiency by electrodynamic tethers," *Acta Astronautica*, Vol. 137, No. 2017, pp.320-333.
doi: 10.1016/j.actaastro.2017.04.025.

[23] Li G., Zhu Z.H., "Precise Analysis of Deorbiting by Electrodynamic Tethers Using Coupled Multiphysics Finite Elements," *Journal of Guidance, Control, and Dynamics*, Vol. 40, No. 12, 2017, pp.3348-3357.
doi: 10.2514/1.G002738.

[24] Du J., Cui C., Bao H., Qiu Y., "Dynamic Analysis of Cable-Driven Parallel Manipulators Using a Variable Length Finite Element," *Journal of Computational and Nonlinear Dynamics*,

Vol. 10, No. 1, 2014, pp.011013-011013-011017.
doi: 10.1115/1.4026570.

[25] Du J., Bao H., Cui C., Yang D., "Dynamic analysis of cable-driven parallel manipulators with time-varying cable lengths," *Finite Elements in Analysis and Design*, Vol. 48, No. 1, 2012, pp.1392-1399.
doi: 10.1016/j.finel.2011.08.012.

[26] Jung W., Mazzoleni A.P., Chung J., "Nonlinear dynamic analysis of a three-body tethered satellite system with deployment/retrieval," *Nonlinear Dynamics*, Vol. 82, No. 3, 2015, pp.1127-1144.
doi: 10.1007/s11071-015-2221-z.

[27] Tang J., Ren G., Zhu W., Ren H., "Dynamics of variable-length tethers with application to tethered satellite deployment," *Communications in Nonlinear Science and Numerical Simulation*, Vol. 16, No. 8, 2011, pp.3411-3424.
doi: 0.1016/j.cnsns.2010.11.026

[28] Li X., Cai Z., "Dynamic Modeling and Simulations of a Tethered Space Solar Power Station," *Journal of Aerospace Engineering*, Vol. 31, No. 4, 2018, pp.04018026.
doi: 10.1061/(ASCE)AS.1943-5525.0000850.

[29] Zhang Y., Wei C., Zhao Y., Tan C., Liu Y., "Adaptive ANCF method and its application in planar flexible cables," *Acta Mechanica Sinica*, Vol.34, No 1. 2017, pp:199-213.
doi: 10.1007/s10409-017-0721-4.

[30] Hong D., Tang J., Ren G., "Dynamic modeling of mass-flowing linear medium with large amplitude displacement and rotation," *Journal of Fluids and Structures*, Vol. 27, No. 8, 2011, pp.1137-1148.
doi: 10.1016/j.jfluidstructs.2011.06.006.

[31] Hong D., Ren G., "A modeling of sliding joint on one-dimensional flexible medium," *Multibody System Dynamics*, Vol. 26, No. 1, 2011, pp.91-106.
doi: 10.1007/s11044-010-9242-7.

[32] Liu J.-P., Cheng Z.-B., Ren G.-X., "An Arbitrary Lagrangian–Eulerian formulation of a geometrically exact Timoshenko beam running through a tube," *Acta Mechanica*, Vol. 229, No.8, 2018, pp:3161-3188.
doi: 10.1007/s00707-018-2161-z.

[33] Li G., Zhu Z.H., Meguid S.A., "Libration and transverse dynamic stability control of flexible

bare electrodynamic tether systems in satellite deorbit," *Aerospace Science and Technology*, Vol. 49, No. 2016, pp.112-129.
doi: 10.1016/j.ast.2015.11.036.